Marine Chemistry 155 (2013) 29–41

Contents lists available at ScienceDirect

Marine Chemistry

journal homepage: www.elsevier.com/locate/marchem

Seasonal and latitudinal variability of the CO_2 system in the western English Channel based on Voluntary Observing Ship (VOS) measurements

P. Marrec *, T. Cariou, E. Collin, A. Durand, M. Latimier, E. Macé, P. Morin, S. Raimund [1], M. Vernet, Y. Bozec

CNRS, UMR 7144, Equipe Chimie Marine, Station Biologique de Roscoff, Place Georges Teissier, 29680 Roscoff, France
UPMC Univ. Paris 06, UMR 7144, Adaptation et Diversité en Milieu Marin, SBR, 29680 Roscoff, France

ARTICLE INFO

Article history:
Received 17 September 2012
Received in revised form 20 May 2013
Accepted 29 May 2013
Available online 5 June 2013

Keywords:
Carbon dioxide
Air–sea CO_2 exchange
Western English Channel
Voluntary Observing Ship

ABSTRACT

We investigated the dynamics of the CO_2 system across the Western English Channel (WEC) between Roscoff (France) and Plymouth (UK) using a Voluntary Observing Ship (VOS). From December 2010 to December 2011, 20 return crossings were carried out to collect a comprehensive dataset of CO_2 system parameters and ancillary data. The hydrographical structure of the water column across the latitudinal transect was investigated at 3 fixed stations: ASTAN (southern WEC, offshore Roscoff), E1 and L4 (northern WEC, offshore Plymouth). Based on these profiles, we defined two provinces, the stratified northern WEC (>49.5°N) and the well-mixed southern WEC (<49.5°N), which were periodically separated by a thermal front. These contrasted hydrographical properties strongly influenced the ecosystem dynamics. Biological production/respiration processes were the main driver of pCO_2 variability during the year except for winter cooling in the northern WEC. The seasonally stratified northern WEC showed enhanced biological activities characterized by an extensive autotrophic phase, which maintained the pCO_2 below the atmospheric equilibrium until early fall and acted as a sink for atmospheric CO_2 at a rate of 1.1 mol C m^{-2} y^{-1}. The permanently well mixed southern WEC was characterized by a shorter autotrophic phase due to a delayed spring phytoplankton growth and an early start of the fall heterotrophic phase, resulting in an annual air–sea CO_2 flux close to equilibrium at a rate of −0.4 mol C m^{-2} y^{-1}. On annual scale, calculation of Net Ecosystem Production (NEP) revealed that surface waters at E1 and ASTAN were both autotrophic at rates of 1.5 mol C m^{-2} y^{-1} and 1.0 mol C m^{-2} y^{-1}, respectively. Our latitudinal approach resolved the discrepancy between the directions of the fluxes in the WEC observed in previous studies by differentiating between the hydrological regions. The combined approach of using data from VOS tracks and fixed coastal observatories stations provided new insights into the control of air–sea CO_2 fluxes in the different provinces of the WEC. This combined approach could be applied in other continental shelf systems where data on the CO_2 system are sparse.

© 2013 Elsevier B.V. All rights reserved.

1. Introduction

Despite the relatively moderate size of continental shelves (7%) compared to the global ocean, these ecosystems play a significant role in the biogeochemical cycle of carbon and in oceanic uptake of atmospheric CO_2 (Walsh et al., 1981; Walsh, 1991). The high biological activity occurring in the marginal seas, ranging from 15% to 30% of oceanic primary production (Gattuso et al., 1998), causes enhanced air–sea CO_2 fluxes (Thomas et al., 2004; Borges, 2005). These marginal seas act as sinks for atmospheric CO_2 whereas near-shore ecosystems act as sources of CO_2 for the atmosphere (Chen and Borges, 2009). Because of the large diversity and heterogeneity of coastal ecosystems, a robust estimation of air–sea CO_2 fluxes in the coastal ocean at the global scale remains a challenge. Recently, Borges et al. (2010) pointed out the need for a global sea surface carbon observing system to unravel inorganic carbon dynamics in coastal ecosystems. Such an observing system would rely on Voluntary Observing Ship (VOS) and time-series measurements of the different parameters of the CO_2 system in seawater for various coastal ecosystems. In this respect, the global estimate of air–sea CO_2 fluxes in costal ecosystems would be improved by a better coverage of these fluxes in different hydrographical regimes.

The Western English Channel (WEC) is part of one of the world's most expended margins, the North-west European continental shelf. This area is characterized by relatively shallow depth and by intense tidal streams with maximum speeds ranging from 0.5 to 2.0 m s^{-1} (maxima for the entire English Channel (EC)) (Reid et al., 1993). The WEC hosts three different hydrographical structures: all year well-mixed, seasonally stratified and thermal front structures. Along the French coast (southern WEC), where the tidal currents are the strongest, the water column remains vertically mixed whereas near the English coast (northern WEC), where tidal streams are less intense, seasonal stratification occurs. Between these two distinct

* Corresponding author. Tel.: +33 665240534.
E-mail address: pmarrec@sb-roscoff.fr (P. Marrec).
[1] Now at: Department of Marine Biogeochemistry, Leibniz-Institute of Marine Science, Kiel, Germany.

0304-4203/$ – see front matter © 2013 Elsevier B.V. All rights reserved.
http://dx.doi.org/10.1016/j.marchem.2013.05.014

structures, a frontal zone oscillates, separating well-mixed and stratified waters (Pingree and Griffiths, 1978). Such water column characteristics are also observed in adjacent seas of the North-west European continental shelf, i.e. in the Irish Sea and in the North Sea (Hill et al., 2008). In this complex hydrographical context, important spatial and temporal variability occur in the dynamics of the CO_2 system (Borges and Frankignoulle, 2003; Padin et al., 2007; Dumousseaud et al., 2010; Kitidis et al., 2012) necessitating high frequency sampling strategy throughout the year for accurate assessment. Previous studies of the CO_2 system in the WEC were either based on longitudinal transects (Borges and Frankignoule, 2003; Padin et al. 2007; Dumousseaud et al., 2010) or a fixed station approach (Kitidis et al., 2012). However, these authors pointed out the need for a latitudinal approach, which would cover each of the hydrographical structures of the WEC and thus better constrain the main drivers of CO_2 system dynamics in the WEC.

In the present study, as part of the European cross-border INTERREG IV project MARINEXUS (Our shared seas: Mechanisms of ecosystem change in the Western Channel) we exploited a VOS route between the French and English coasts (Fig. 1), which crosses the different hydrographical structures of the WEC described above. Bi-monthly sampling on the *Armorique* ferry (Brittany Ferries) provided a comprehensive new dataset of the CO_2 system and ancillary data in the WEC. Furthermore, data were also collected as part of the Western Channel Observatory of Plymouth (NERC National Capability of the Plymouth Marine Laboratory and Marine Biological Association) and the French network for observation of the coastal ocean (SOMLIT) at three fixed stations, one off the French coast (ASTAN, all year well-mixed) and two off the English coast (E1, L4, seasonally stratified), to determine the physical structure of the water column in these contrasting systems.

Based on this dataset, we investigated the carbonate system dynamics along a latitudinal gradient for the first time in the WEC. In the present paper, we first present the physical characteristics of the different WEC provinces and the spatio-temporal distribution of the carbonate system and ancillary data in these provinces. We then discuss the processes controlling the spatial distribution and the temporal variability of surface water partial pressure of CO_2 (pCO_2) and air–sea CO_2 fluxes across the WEC. Finally, based on the dissolved inorganic carbon (DIC) data and air–sea CO_2 flux calculations, we estimate the net ecosystem production (NEP) in the well-mixed and seasonally stratified systems and relate it to the trophic status of each system.

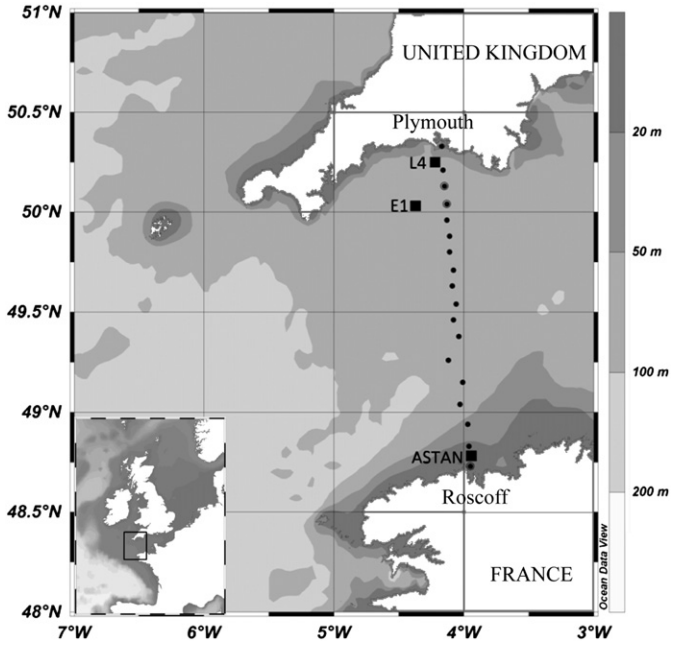

Fig. 1. Map and bathymetry of the study area with the locations of the 18 stations along the ferry track and location of the fixed stations ASTAN, E1 and L4.

2. Material and methods

2.1. Surface measurements on the VOS line

Data were collected from the 22nd of December 2010 to the 19th of December 2011 across the Western English Channel between Roscoff (France, 48°43′38 N 3°59′03E) and Plymouth (United Kingdom, 50°22′ 12 N 4°08′31E) (Fig. 1). Transects were performed every two weeks on board the *Armorique* ferry (Brittany Ferries). A -4H- JENA engineering Ferry Box system was installed at the engine room level on the ferry in 2010. The Ferry Box pumped seawater at 4 m depth with a high flow rate to avoid warming of seawater in the water column circuit. The pump was operational only when the ferry was sufficiently far from the harbors to avoid introducing particle-rich waters into the system. A Sea Bird SBE 38 temperature sensor recorded the in-situ seawater temperature with a precision of 0.01 °C whereas a Sea Bird SBE 45 thermosalinograph recorded the temperature and salinity inside the seawater circuit of the Ferry Box with precisions of 0.01 °C and 0.001, respectively. During the year of study, we undertook 20 return crossings between Roscoff and Plymouth and sampled a total of 353 surface stations in the WEC (Table 1). During each cruise, 18 water samples were sampled from the Ferry Box seawater circuit for the determination of dissolved oxygen (DO), dissolved inorganic carbon (DIC), total alkalinity (TA), nutrients, chlorophyll-*a* (Chl-*a*) and salinity. Discrete salinity samples were collected to calibrate the autonomous SBE 45 sensor. Discrete samples were measured on a portasal salinometer at the SHOM (Service Hydrographique et Oceanographique de la Marine) with a precision of 0.002 and were in good agreement with the SBE 45 measurements ($Salinity_{SBE45} = Salinity_{SHOM} \times 0.99$, $n = 270$, $r^2 = 0.96$). O_2 samples (280 mL brown glass bottles) were poisoned with 1.7 mL of manganese chlorate (600 g L^{-1}) immediately after sampling; samples were kept in the dark in a water bath and analyzed within a week of sampling. DO concentrations were determined by the Winkler method using a potentiometric end-point determination with an estimated accuracy of 0.5 μmol L^{-1}. The oxygen saturation level (DO%) was then calculated according to Weiss (1970) from the observed DO and the DO at saturation using the in-situ temperature and salinity. DIC and TA were collected in 100 mL and 250 mL borosilicate glass bottles, respectively, poisoned with 100 μL of $HgCl_2$, and analyzed within a week of sampling. DIC was determined with an AIRICA system (Marianda Inc.) after acidification of a 2.3 mL aliquot with phosphoric acid, extraction by a carrier gas (N_2) and detection with an IR detector LICOR-7000. TA was measured with a TA-ALK 2 system (Appolo SciTech.) by the Gran electrotitration method on 25 mL aliquots. The accuracies of DIC and TA measurements were determined with Certified Reference Materials (CRM) provided by A. G. Dickson, Scripps Institution of Oceanography (Batch 92). CRM

Table 1
Dates of transects Roscoff–Plymouth–Roscoff between the 22nd of December 2010 and the 19th December 2011 and number of samples collected for each parameters studied.

Date	Number of samples	Date	Number of samples
22 Dec 10	18	29 Jun 11	18
17 Feb 11	14	11 Jul 11	18
3 Mar 11	18	27 Jul 11	18
15 Mar 11	17	17 Aug 11	18
29 Mar 11	18	31 Aug 11	18
13 Apr 11	18	14 Sep 11	18
30 Apr 11	18	8 Oct 11	18
14 May 11	18	22 Oct 11	18
30 May 11	18	8 Nov 11	18
15 Jun 11	18	19 Dec 11	18

standards were measured at the start and at the end of each day of analysis and every 10 samples during the runs. Accuracies of the DIC and TA measurements were 1.5 μmol kg^{-1} and 3 μmol kg^{-1}, respectively. To determine chlorophyll-*a* concentrations (Chl-*a*), 0.5 L of seawater was filtered through glass-fiber filters (Whatman GF/F) and immediately frozen. Samples were extracted in 5 mL of acetone, acidified with an HCl solution and Chl-*a* concentrations were measured using a fluorometer (model 10 analog fluorometer Turner Designs) according to EPA (1997), with an estimated accuracy of 0.05 μg L^{-1}.

2.2. Water column measurements at fixed stations

During the same period, we acquired water column profiles of temperature and salinity from three fixed stations representative of the physical structure of the WEC (homogenous vs. stratified). The ASTAN station (48°46′40 N 3°56′15 W, bottom depth of 60 m), situated 3.5 km north of Roscoff (Fig. 1), is representative of a well mixed water column system as described by Wafar et al. (1983) and was visited every two weeks as part of the Roscoff Coastal Observatory (SOMLIT). At ASTAN, CTD profiles were obtained with a Seabird SBE 19+, with precisions for temperature and computed salinity of 0.005 °C and 0.002, respectively. Station E1 (50.03°N 4.37°W; depth 75 m) and L4 (50.25°N 4.22°W; depth 50 m), located approximately 38 km and 12 km off Plymouth (Fig. 1), were representative of seasonally stratified open shelf seas and coastal waters of the WEC, respectively (Smyth et al., 2010). Measurements were undertaken by the Western Channel Observatory (NERC National Capability of the Plymouth Marine Laboratory and Marine Biological Association), weekly at coastal station L4 and fortnightly at open shelf station E1. CTD profiles were obtained with a Seabird SBE 19+ and provided the same precisions as given above for temperature and salinity. DIC and TA were not directly sampled at the fixed stations ASTAN and E1. In the following discussion, for these two parameters we refer to data sampled from the VOS line in the vicinity of fixed stations ASTAN end E1.

2.3. Calculation of the partial pressure of CO_2 and air–sea CO_2 fluxes

The seawater partial pressure of CO_2 (pCO_2) were calculated from TA, DIC, temperature, salinity and nutrients concentrations with the CO2SYS program (Pierrot et al., 2006) using the equilibrium constants of CO_2 proposed by Mehrbach et al. (1973), refitted by Dickson and Millero (1987) on the seawater pH scale. The computed values of pCO_2 from DIC and TA have uncertainty of ±5.8 μatm (Zeebe and Wolf-Galdrow, 2001). Atmospheric pCO_2 ($pCO_{2\ air}$) was calculated from the CO_2 molar fraction (xCO_2) at the Mace Head site (53°33′N 9°00′W, southern Ireland) of the RAMCES network (Observatory Network for Greenhouse Gases) and from the water vapor pressure (pH_2O) using the Weiss and Price (1980) equation. Atmospheric pressure (Patm) in the middle of the WEC (49°50′N, 4°00′W) was obtained from the NCEP/NCAR re-analysis project.

The fluxes of CO_2 across the air–sea interface (F) were computed from the pCO_2 air–sea gradient ($\Delta pCO_2 = pCO_{2\ water} - pCO_{2\ air}$, μatm) according to:

$$F = k \times \alpha \times \Delta pCO_2 \quad (1)$$

where k is the gas transfer velocity (m s^{-1}) and α is the solubility coefficient of CO_2 (mol atm^{-1} m^{-3}) calculated after Weiss (1970). The exchange coefficient k was computed as a function of wind speed with the algorithm given by Nightingale et al. (2000) established in the Southern Bight of the North Sea (SBNS). The SBNS and the WEC present similar environmental characteristics: these two shallow continental shelves are both close to land with high tidal currents controlling the physical structure of the water column. Wind speed data corrected to 10 m height were obtained from the NCEP/NCAR re-analysis project (Kalnay et al., 1996) provided by the NOAA-ESRL Physical Sciences Division (Boulder, CO, USA, http://wwww.esrl.noaa.gov/psd/). Four time daily wind speed were extracted on the north (>49.5°) and South (<49.5°) parts of the transect. The data were averaged over two week periods centered on the date of each crossing (Table 1). To estimate the range of the air–sea CO_2 fluxes obtained with other k-wind parameterizations, the fluxes were also computed using the formulation of Wanninkhof and McGillis (1999) for short term (<1 day) and long term (>1 month) winds. These ranges are given for annual fluxes in Table 5 and are represented by the error bars on Fig. 6.

2.4. Calculation of the net ecosystem production

The net ecosystem production (NEP) quantifies the metabolic status of an ecosystem and corresponds to the difference between organic matter production and mineralization. In other terms, it is the difference between gross primary production (GPP) and ecosystem respiration (R). An ecosystem is deemed net autotrophic when production of organic matter is larger than its consumption (NEP > 0). In heterotrophic systems, respiration processes predominate (NEP < 0) and such systems require external organic carbon inputs (Odum, 1956). Gazeau et al. (2005) described and compared several methods to assess NEP for European coastal zones and argued that such assessment can be performed from the DIC budget. Here, NEP was computed from the temporal DIC variations between two cruises using the method employed by Bozec et al. (2006), Schiettecatte et al. (2007) and Borges et al. (2008) according to the following equation:

$$NEP = (DIC_1 - DIC_2) \times d/\Delta t - F \quad (2)$$

where DIC_1 and DIC_2 are the mean values in mmol m^{-3} during two consecutive cruises, d is the Mixed Layer Depth (MLD) in m, Δt is the time interval in days between the two cruises and *F* is the mean air–sea CO_2 flux for the two cruises. This calculation was performed on data from the vicinity of ASTAN station for the entire water column and on data from the vicinity of E1 station for the MLD determined from the CTD profiles (Table 3). MLD was defined as the shallowest depth corresponding to a temperature or density difference with the surface water higher than δT = 0.5 °C and δDens = 0.125 (Monterey and Levitus, 1997).

NEP assessments were not performed at L4 due to freshwater inputs, which strongly influenced the carbonate system properties on time scales less than 2 weeks. For the other stations, the computations were carried out considering that the relatively low Δt used (two weeks) does not exceed the flushing time in the area, which ranges from 30 to 90 days in the English Channel (Delhez et al., 2004). Such an approach implies the assumption that air–sea CO_2 exchanges, GPP and R are the main drivers of the CO_2 dynamics. According to Southward et al. (2005) (and references therein), diatoms are the main phytoplankton group during the spring and late summer–early fall blooms (influencing the GPP), whereas dinoflagellates dominate during summer in the WEC. Calcifying species such as coccolithophores can be present in the WEC (Garcia-Soto et al., 1995; Southward et al., 2005; Widdicombe et al., 2010). Satellite images from MODIS-Aqua Particulate Inorganic Carbon (PIC) algorithms (http://oceancolor.gsfc.nasa.gov) revealed that during our year of study coccolithophore blooms were present in the surface waters at E1 in early June and between 49.6°N and 49.9°N during one week at the end of July. These observations were supported by phytoplankton class time-series data at station L4 (Western Channel Observatory), which confirmed the presence of coccolithophore bloom at this station. The impacts of these blooms and of benthic calcification on the seasonal and annual NEP computation are discussed

below. For this NEP computation, the net advective input/output of DIC between two cruises must be assumed to be constant. The relatively short time intervals of the computation (two weeks) allow make this assumption reasonable to accept. However, short-scale eddies might induce gradients of the carbonate system in the area, which are difficult to quantify in this study but add to the uncertainty of our NEP computations.

3. Results

3.1. Hydrographical setting

3.1.1. Surface waters

In the following sections, we define spring from the 21st of March to the 21st of June, summer from the 22nd of June to the 22nd of September, fall from the 23rd of September to the 21st of December and winter from the 22nd of December to the 20th of March. Sea surface temperature (SST) in the WEC followed classical dynamics with a warming of surface waters from spring to the end of summer and a cooling from early fall to winter (Fig. 2a and Table 2). Coolest SST was recorded in February (8.3 °C), whereas warmest SST occurred at end of July and beginning of August (17.1 °C) resulting in an annual temperature amplitude of approximately 9 °C. Winter surface waters were cooler in the northern compared to the southern WEC. Analysis of individual transects of SST (Fig. 3) showed that thermal fronts occurred from mid-May to mid-September and fluctuated between 49.1°N and 49.7°N during these four months. During winter and spring, minimum SST was recorded near the coast at a latitude north of 50°N due to the discharge of freshwater from the Plymouth rivers. These freshwater inputs lowered the salinity (<35.30) of surface waters in the area throughout almost all of the year (Fig. 2b). In the southern part of the WEC, from February to June, low salinity (<35.30) surface waters were also recorded and salinity dropped below 35.10 (Table 2). According to Kelly Gerreyn et al. (2006), low saline waters from the Loire plume can reach the southern part of the WEC and these coastal waters are also influenced by freshwater discharges from local Britanny rivers. The highest salinity (>35.50) values were recorded during fall in the entire WEC except near Plymouth where freshwater inputs still occurred.

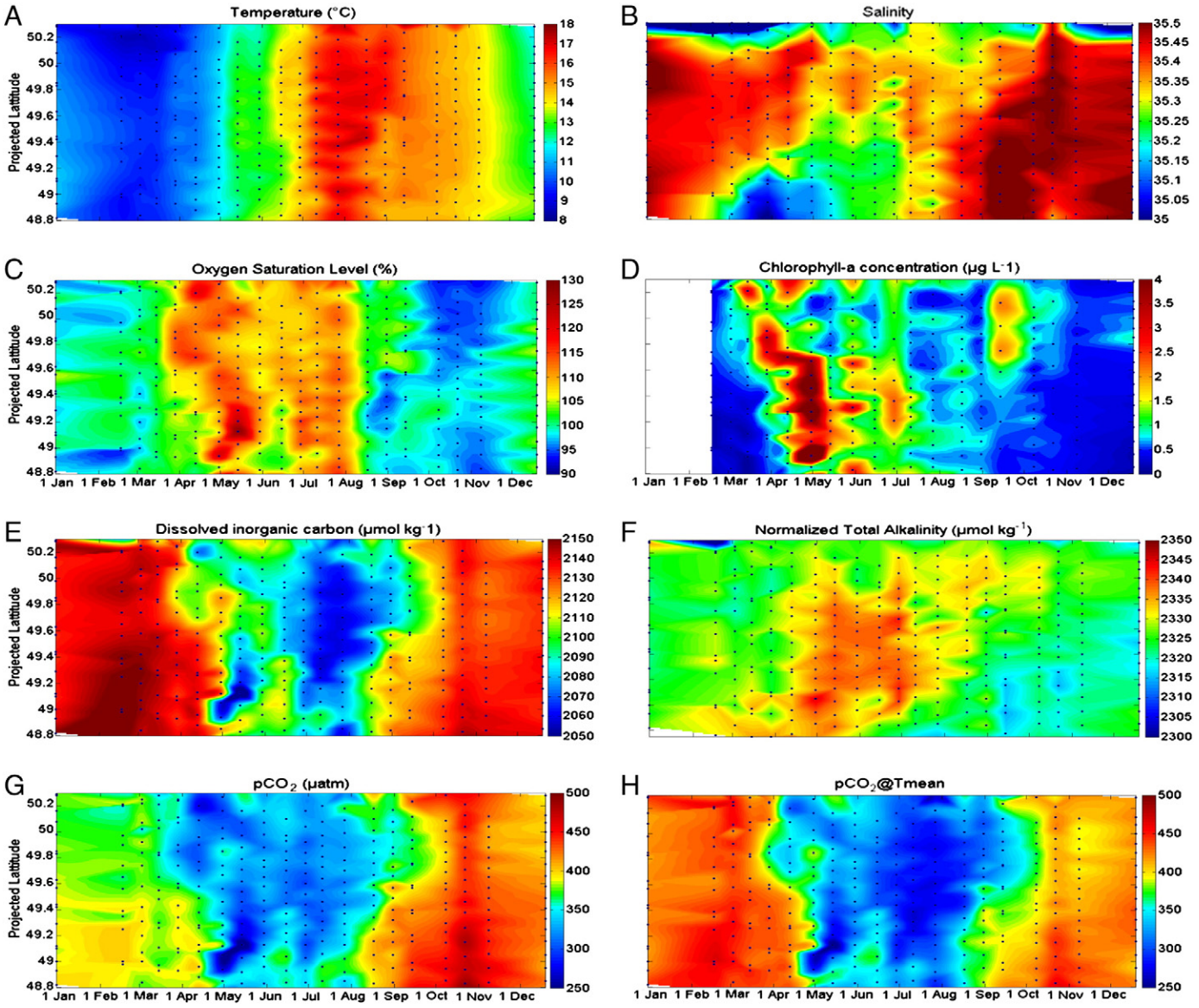

Fig. 2. Surface distribution for the year 2011 of (A) temperature (°C), (B) salinity, (C) DO%, (D) Chl-*a* (mg L^{-1}), (E) DIC (in µmol kg^{-1}), (F) normalized TA after Friis et al. (2003) (in µmol kg^{-1}), (G) pCO_2 (in µatm) and (H) pCO_2 normalized at the mean temperature of 13.1 °C (pCO_2@13.1 °C) (in µatm) in the WEC between Roscoff and Plymouth.

Table 2
Seasonal means of SST (C), SSS. DO%, Chl-*a* (μg L^{-1}), DIC (μmol kg^{-1}), TA (μmol kg^{-1}), pCO_2 (μatm) and wind speed (m s^{-1}) in the southern (<49.5 N) and the northern (>49.5 N) WEC and for the fixed stations ASTAN, E1 and L4 based on the VOS line measurements. The range of values measured each season is given by the numbers in brackets. Each season is defined as follows: winter (22nd of December to the 20th of March), spring (from the 21st of March to the 21st of June), summer (from the 22nd of June to the 22nd of September) and fall (from the 23rd of September to the 21st of December).

Region	Season	SST	SSS	DO%	Chl-*a*	DIC	TA	pCO_2	Wind speed
ASTAN	Winter	9.9 (9.3–11.2)	35.13 (35.04–35.29)	98 (92–102)	0.2 (0.1–0.4)	2145 (2138–2155)	2339 (2333–2343)	387 (375–399)	5.9 (0.6–11.7)
	Spring	12.2 (10.1–14.4)	35.11 (34.99–35.27)	109 (102–130)	1.6 (0.2–7.1)	2110 (2067–2140)	2337 (2327–2344)	355 (306–402)	6.8 (5.0–10.1)
	Summer	15.3 (14.3–16.4)	35.35 (35.16–35.50)	106 (97–124)	0.9 (0.5–1.9)	2100 (2062–3131)	2334 (2324–2343)	392 (343–453)	4.8 (2.1–8.3)
	Fall	14.1 (12.2–15.2)	35.47 (35.41–35.58)	98 (95–104)	0.4 (0.1–0.5)	2140 (2133–2149)	2337 (2331–2345)	457 (497–410)	9.4 (7.2–12.4)
South	Winter	10.2 (9.5–11.3)	35.35 (35.19–35.40)	99 (90–102)	0.3 (0.1–0.6)	2143 (2133–2155)	2339 (2335–2346)	388 (374–401)	6.4 (0.6–11.7)
	Spring	11.9 (10.2–13.8)	35.24 (35.11–35.36)	109 (102–128)	1.9 (0.6–4.6)	2108 (2040–2142)	2343 (2326–2350)	341 (241–391)	7.0 (4.7–10.1)
	Summer	15.5 (14.2–17.1)	35.35 (35.21–35.49)	106 (95–115)	1.0 (0.6–2.3)	2089 (2058–2121)	2342 (2334–2351)	361 (299–431)	5.1 (2.1–8.4)
	Fall	14.1 (12.4–15.1)	35.48 (35.34–35.51)	99 (96–104)	0.4 (0.2–0.7)	2132 (2122–2140)	2336 (2331–2340)	439 (413–481)	9.7 (8.5–12.4)
North	Winter	9.97 (9.4–10.9)	35.42 (35.41–35.44)	99 (85–105)	0.7 (0.4–0.9)	2139 (2133–2145)	2339 (2334–2343)	375 (358–384)	6.0 (1.8–8.9)
	Spring	12.2 (10.2–14.4)	35.34 (35.25–35.43)	110 (106–115)	1.5 (0.6–3.6)	2102 (2080–2134)	2344 (2334–2350)	329 (302–372)	7.4 (3.7–11.0)
	Summer	16.0 (14.2–17.0)	35.33 (35.24–35.41)	107 (95–116)	0.9 (0.5–2.0)	2076 (2059–2114)	2342 (2335–2351)	342 (300–407)	4.7 (0.9–8.4)
	Fall	14.1 (12.1–15.0)	35.47 (35.41–35.50)	98 (94–105)	0.6 (0.4–0.9)	2127 (2117–2138)	2340 (2335–2345)	419 (397–442)	9.7 (6.3–11.6)
E1	Winter	9.3 (8.8–10.5)	35.34 (35.24–35.41)	100 (90–108)	1.0 (0.8–1.4)	2137 (2121–2144)	2337 (2332–2340)	364 (348–383)	6.3 (3.0–8.8)
	Spring	11.4 (9.1–14.0)	35.32 (35.24–35.41)	110 (105–115)	1.0 (0.6–1.3)	2103 (2085–2135)	2339 (2334–2345)	330 (305–357)	7.3 (3.7–10.0)
	Summer	16.1 (14.7–16.7)	35.30 (35.24–35.35)	106 (102–112)	0.9 (0.5–2.1)	2082 (2066–2100)	2342 (2340–2345)	352 (328–378)	4.9 (2.6–7.1)
	Fall	13.8 (12.1–14.9)	35.42 (35.38–35.46)	98 (94–108)	0.7 (0.5–1.0)	2129 (2121–2136)	2342 (2340–2344)	413 (400–449)	9.8 (9.2–11.1)
L4	Winter	8.9 (8.3–10.3)	34.38 (31.35–35.19)	101 (96–110)	1.0 (0.3–2.9)	2124 (2025–2147)	2313 (2169–2339)	369 (326–393)	6.0 (1.8–8.8)
	Spring	11.2 (9.3–13.7)	35.12 (34.51–35.30)	110 (104–119)	1.4 (0.6–2.9)	2103 (2074–2133)	2333 (2326–2345)	333 (272–367)	7.1 (4.4–11.0)
	Summer	15.6 (14.4–16.3)	35.11 (34.68–35.31)	104 (94–113)	1.0 (0.6–1.6)	2091 (2070–2121)	2336 (2326–2342)	375 (322–543)	4.9 (0.9–7.1)
	Fall	13.8 (11.6–14.9)	35.10 (34.35–35.46)	95 (93–101)	0.6 (0.4–0.9)	2131 (2116–2138)	2333 (2312–2343)	434 (392–471)	9.6 (7.8–11.1)

3.1.2. Water column properties

Fig. 4 shows the annual variations of temperature and salinity in the water column at stations ASTAN (southern WEC, offshore Roscoff), E1 and L4 (northern WEC, offshore Plymouth). These profiles show that thermal stratification occurred during spring and summer in the northern part of the WEC at station E1 and L4. The MLD (mixed layer depth) at E1 ranged between 15 m and 25 m depth, with an average depth of 20 m from April to October (Table 3). Salinity at this open shelf station ranged between 35.20 and 35.50. Freshwater inputs often decreased salinity at the same latitude and in the vicinity of station E1 compared to the rest of the northern WEC. The L4 station was even more influenced by river inputs than at the latitude of E1. From the salinity and temperature profiles, we found that the MLD at L4 ranged between 10 m and 30 m, with an average value of 17 m (Table 3). Stratification occurred almost all year round at station L4 due to these freshwater inputs which decreased the surface water density. Salinity decreased to 34.80 from January to April and fell to 34.50 in December 2011. Thermal stratification also occurred from April to October at station L4. At ASTAN, hydrographical profiles showed that the water column was well mixed throughout the year. Temperatures ranged between 8.8 °C (in winter) and 15.7 °C (in summer) (Table 3). The lowest salinity values were recorded at the end of winter and during spring (35.05 and 35.04 respectively) whereas salinity increased continuously from late spring to early fall to reach values around 35.50.

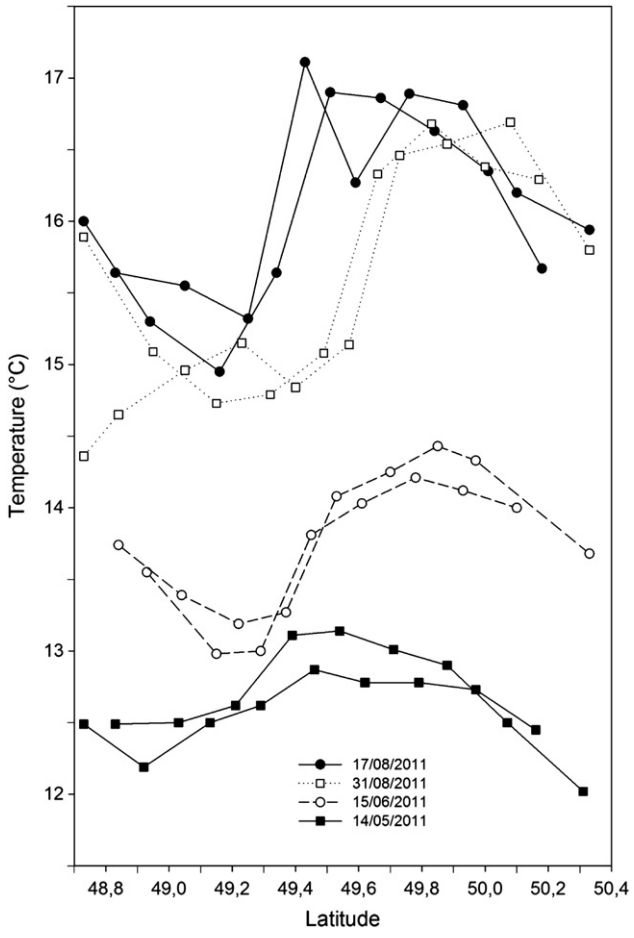

Fig. 3. Latitudinal variations of temperature (°C) across the WEC between Roscoff and Plymouth on the 14th of May 2011 (filled squares), the 15th of June 2011 (empty circles), the 17th of August 2011 (filled circles) and the 31st of August 2011 (empty squares).

Based on these profiles and on the SST data from the transects, we distinguished two main hydrographical provinces in the WEC: the seasonally stratified waters of the northern WEC (>49.5°N) and the all-year mixed waters of the southern WEC (<49.5°N). These two regions were periodically separated by a thermal front, which oscillated around the latitude of 49.5°N as previously described by Pingree and Griffiths (1978). The limit of 49.5°N between these two provinces was chosen arbitrarily from the average position of the front observed during the period of study.

3.2. Surface distributions of DO% and Chl-a

In the northern WEC, winter values of DO% were close to atmospheric equilibrium in a homogeneous water column (Fig. 4) mixed by relatively high wind speeds (Fig. 2c and Table 2). Hydrographical conditions and the low winter irradiance did not allow phytoplankton development and Chl-*a* values remained low (<1 μg L^{-1}) during winter (Fig. 2d and Table 2). Chl-*a* started to increase in March in this northern region to reach values around 3 μg L^{-1} associated to DO% above atmospheric equilibrium. In the following months, surface water Chl-*a* decreased

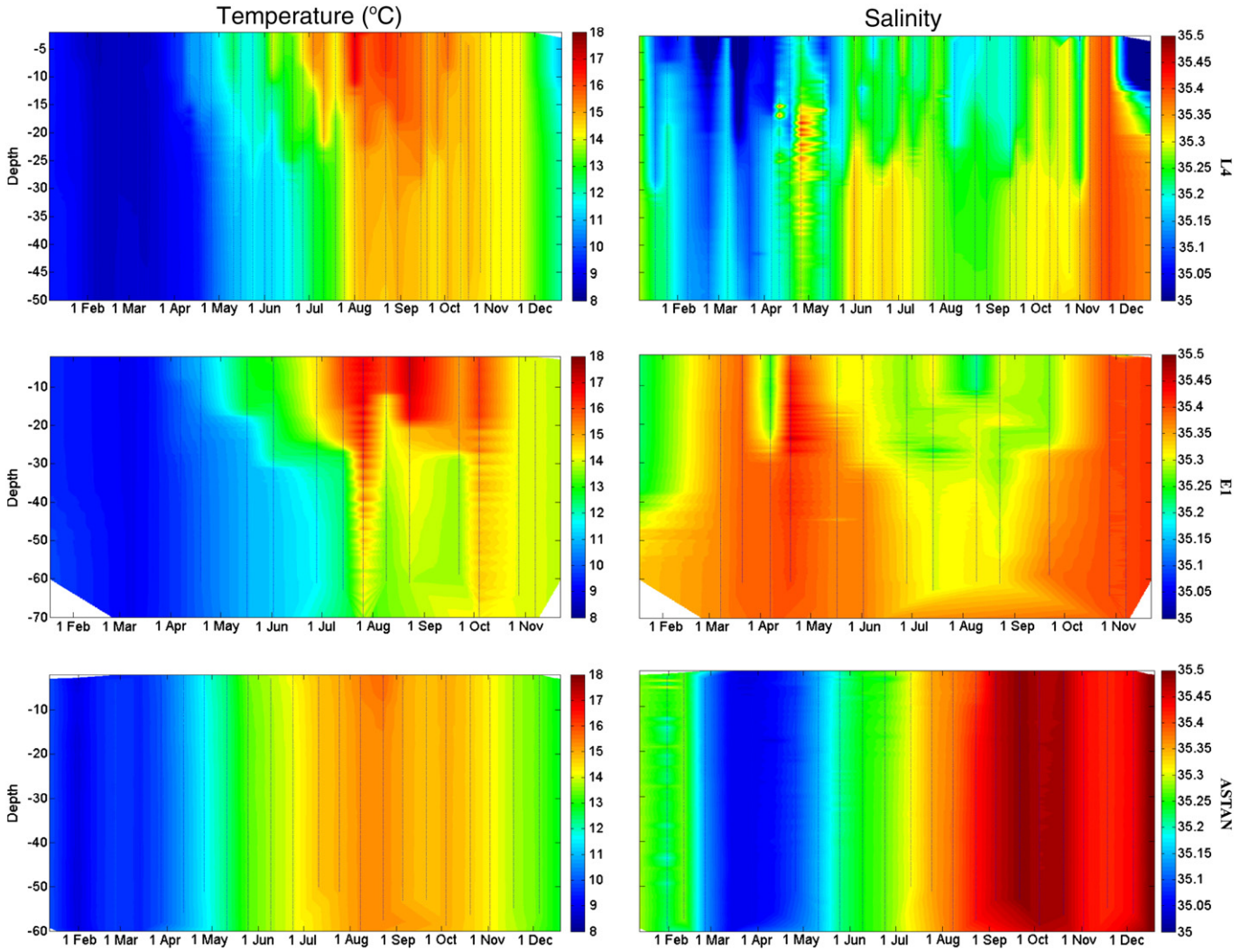

Fig. 4. Profiles of temperature (left) and salinity (right) during the year 2011 at fixed stations ASTAN, E1 and L4.

down to 1 μg L^{-1} (except in early July when Chl-*a* exceeded 1.5 μg L^{-1}), whereas DO% remained above atmospheric equilibrium. At the same time, closer to the coast, Chl-*a* concentrations remained higher and were associated with surface water DO% above atmospheric equilibrium with an average value of 105%. Around mid-September, a late phytoplankton bloom occurred between 49.7°N and 50.2°N with Chl-*a* reaching 2 μg L^{-1}. The DO% started to decrease towards atmospheric equilibrium before this phytoplankton bloom, but increased back up to 105% during the bloom. After this late summer bloom, Chl-*a* fell below 1 μg L^{-1} until December. During October and early November the lowest values of DO% were recorded (between 90% and 100%) before reaching atmospheric equilibrium with re-homogenization of the water column during winter.

In the southern WEC, winter values of DO% were close to atmospheric equilibrium and Chl-*a* remained low (Table 2 and Fig. 2c and d) in a well-mixed water column. Compared to the northern WEC, Chl-*a* started increasing approximately 1 month later, around mid-April. This increase in Chl-*a* was associated with DO% values above atmospheric equilibrium of approximately 105%, lower than in the northern WEC at the same period (Table 2, Fig. 2c and d). Around the 30th of April, at latitudes below 49.5°N, an important phytoplankton bloom occurred. During this event, Chl-*a* values increased above 2.5 μg L^{-1} between Roscoff and the latitude 49.5°N with maximal concentrations over 4 μg L^{-1}. Surface waters DO% increased significantly above atmospheric equilibrium inside the bloom with values reaching 120% on the 30th of April transect, remaining very high during the next crossing two weeks later. In southern WEC surface waters, Chl-*a* remained relatively high (>1 μg L^{-1}) with several peaks of Chl-*a* until early July. Similarly to the northern WEC, surface waters in the southern WEC were still over-saturated with oxygen in August. However, surface water DO% decreased and fell below atmospheric equilibrium between 49.1°N and 49.5°N at the end of August, nearly 1 month earlier than in the northern WEC. From the end of summer to winter, Chl-*a* decreased continuously to reach values of

Table 3
Seasonal means of temperature (C), salinity and MLD (m) measured and computed from CTD profiles at the fixed stations ASTAN, E1 and L4. The range of values measured each season is given by the numbers in brackets.

Station	Season	Temperature (°C)	Salinity	MLD (m)
ASTAN	Winter	9.5 (8.8 9.9)	35.19 (35.05 35.30)	
	Spring	12.0 (10.0 13.8)	35.14 (35.04 35.25)	
	Summer	14.9 (14.1 15.7)	35.38 (35.23 35.49)	
	Fall	14.1 (12.7 15.0)	35.46 (35.41 35.52)	
E1	Winter	9.3 (9.0 9.8)	35.34 (35.22 35.39)	
	Spring	10.6 (9.3 13.1)	35.37 (35.25 35.47)	19 (17.3 24)
	Summer	14.3 (11.6 17.2)	35.30 (35.21 35.33)	16.8 (11.8 26.8)
	Fall	14.3 (13.6 16.2)	35.38 (34.05 35.41)	21
L4	Winter	8.8 (8.5 9.4)	35.15 (34.81 35.29)	11.6 (6.7 16.5)
	Spring	10.8 (8.8 13.9)	35.21 (35.04 35.43)	18.0 (9.0 32.3)
	Summer	14.4 (12.1 17.0)	35.26 (35.16 35.32)	17.4 (8.3 28.8)
	Fall	14.5 (14.1 15.6)	35.32 (35.16 35.40)	10.3 (10.0 10.5)

0.5 μg L^{-1}. DO% measured in the southern WEC ranged from 97% to 103% in early fall. DO% decreased at the end of fall, ranging from 90% to 100% with average values around 97%, before reaching equilibrium during winter.

Thus, our arbitrary separation at 49.5°N based on water mass properties allowed observation of very contrasting dynamics regarding phytoplankton growth and DO% distribution, which were related to the different hydrographical structures.

3.3. Surface distributions of CO_2 system parameters

3.3.1. Total alkalinity

TA values across the WEC ranged from 2169 μmol kg^{-1} to 2351 μmol kg^{-1} (Table 2). During winter, the longitudinal variability of TA along the transects showed an average value of 2339 μg kg^{-1} in the northern and the southern WEC and minima of 2169 μg kg^{-1} observed near the English coast associated with freshwater inputs (salinity below 35.00). In mid-March, lower values of TA down to 2330 μg kg^{-1} were measured in the south (<49.3°N). This lower TA was related to the presence of less saline waters (<35.20), which might have resulted either from local river discharge or from surface waters from the Loire plume as observed by Kelly Gerreyn et al. (2006). Fig. 2f shows the distribution of normalized TA (nTA) according to Friis et al. (2003). This normalization allowed us to remove the effect of salinity variation on TA and thus revealed the effects of biogeochemical processes on TA. During spring, nTA increased up to 2335 μg kg^{-1} in the WEC whereas coastal nTA in the northern WEC remained low during this period. Interestingly, high Chl-*a* values were always followed by an increase of nTA. From the end of July to fall, TA and nTA decreased to TA values ranging from 2330 to 2340 μmol kg^{-1} (Table 2) and to nTA values ranging from 2315 to 2330 μmol kg^{-1} (Fig. 2f), except during two weeks after the late summer bloom in the northern WEC. The control of freshwater inputs vs phytoplankton blooms on the spatio-temporal variability of TA is discussed in Section 4.1.

3.3.2. Dissolved inorganic carbon

DIC distribution in the WEC (Fig. 2e) followed a clear temporal dynamics. During fall and winter, DIC concentrations were high with values ranging from 2130 to 2155 μmol kg^{-1}. Maximum values of DIC were measured during winter, mostly in the southern part of the WEC when SST was lowest and when biological activity was negligible (Table 2). During spring and summer, much lower DIC concentrations (<2100 μmol kg^{-1}) were recorded. A minimum of 2040 μmol kg^{-1} was recorded in mid-May in the southern WEC just after the main bloom described above in Section 3.2 (Fig. 2d). The dynamics of DIC differed in the northern and southern WEC. DIC concentrations started decreasing one month earlier in the north (end of March) compared to the south. In the southern WEC, DIC concentrations reached 2040 μmol kg^{-1} in mid-May during the major phytoplankton bloom, whereas DIC values did not fall below 2080 μmol kg^{-1} before mid-June in the northern WEC. After this event, DIC increased again to reach a value of 2110 μmol kg^{-1}. North of 49.6°N, DIC remained below 2090 μmol kg^{-1} until mid-September, whereas south of 49.3°N, DIC values below 2090 μmol kg^{-1} were recorded until early August. Finally, DIC concentrations increased during fall and winter to reach values above 2130 μmol kg^{-1} in both regions.

3.3.3. Partial pressure of CO_2

Fig. 2g shows the spatial and temporal distribution of pCO_2, computed from TA and DIC, between Roscoff and Plymouth over the year 2011. Surface water pCO_2 ranged from 241 μatm during spring (mid-May) to 496 μatm in early fall (mid-October) (Table 2). From winter to early spring, before the first phytoplankton bloom occurred, pCO_2 ranged between 350 and 400 μatm across the transects with the lowest values observed in the cooler surface waters of the northern WEC. When spring blooms started, the drawdown of pCO_2 showed the same trend as that of DIC, starting firstly in the northern WEC and one month later in the southern WEC. After the first bloom, surface water pCO_2 decreased to 272 μatm in the northern WEC, and to 241 μatm in the southern WEC (Table 2). The same spatio-temporal distribution as that of DIC was observed for pCO_2 across the WEC during summer. In the northern WEC, the summer pCO_2 ranged from 300 to 370 μatm until mid September, whereas this range of pCO_2 values only persisted until early August in the southern WEC. During fall, the surface water pCO_2 increased above atmospheric equilibrium to reach a value over 450 μatm in the south and values between 430 and 450 μatm in the north. After the fall maximum, surface water pCO_2 decreased to a value close to atmospheric equilibrium in the south and below atmospheric equilibrium in the north during winter.

4. Discussion

4.1. Latitudinal dynamics of the carbonate system in the WEC

Previous studies of carbonate system dynamics in the English Channel were based either on longitudinal transects by Borges and Frankignoulle (2003), Padin et al. (2007) and Dumousseaud et al. (2010), or on fixed stations at E1 and L4 by Kitidis et al. (2012). A similar range of values for DIC/TA (Dumousseaud et al., 2010; Kitidis et al., 2012) and pCO_2 (Table 4) was recorded in our dataset as those reported in these studies. However, compared to previous studies, our high latitudinal coverage allowed a new separation of the WEC with respect to the distributions of carbonate system parameters and ancillary data. The relatively high temporal frequency employed in this study allowed distinction of temporal differences in carbonate system variability between the two provinces. As mentioned in Section 3, DIC and pCO_2 variability were closely related to DO% and Chl-*a* distributions. After the spring bloom in the northern WEC, Chl-*a* remained low during summer, but DO% was above atmospheric equilibrium and DIC and pCO_2 remained relatively low (under 2090 μmol kg^{-1} and 350 μatm, respectively). These observations suggest the presence of a sub-surface phytoplankton bloom above the thermocline after nutrient depletion in the surface layer, as reported previously by Southward et al. (2005) and by Smyth et al. (2010). The water column was always mixed during the same period in the southern WEC. A subsurface Chl-*a* maximum did not occur in this region and phytoplankton was present until total nutrient depletion throughout the water column (data not shown) and were associated with lower values of pCO_2/DIC. An additional difference between the northern and the southern WEC was the late phytoplankton bloom that occurred in the northern province in late summer. This event delayed the increase of DIC and pCO_2 due to organic matter remineralization. These observations suggested a strong control of biological processes on DIC/pCO_2 variability with temporal decoupling between the two provinces.

Table 4
Seasonal range of pCO_2 values (μatm) observed in this study across the WEC and reported by Borges and Frankignoulle (2003) (B & F), Padin et al. (2007) (P et al.) and Dumousseaud et al. (2010) (D et al.) in thre EC and Kitidis et al. (2012) (K et al.) at stations E1 and L4. These pCO2 values were extracted from graphs of these studies and they represent the approximate range of pCO_2 values measured during each season.

	Winter	Spring	Summer	Fall
pCO2, WEC, this study	350–400	240–315	300–370	430–495
pCO2, EC (B & F)	360–390	300–340	200–350	400
pCO2, EC (P et al.)	370	290–350		375–425
pCO2, EC (D et al.)	400–430	310–340	340–350	390–440
pCO2, E1/L4 (K et al.)	350–400	290–310	300–330	400

For TA, as shown in Section 3.3, coastal freshwater inputs were significant drivers of latitudinal variability. In addition, TA can be controlled by production (decrease of TA) and dissolution (increase of TA) of calcium carbonate (Wolf-Gladrow et al., 2007). As mentioned in Section 2.4, coccolithophore blooms occurred in the northern WEC as revealed by MODIS-Aqua satellite images and data of flow cytometry at fixed station L4 (Western Channel Observatory). On these satellite images, we observed a coccolithophore bloom between 49.9°N and 50.2°N, in early June and a second one at the end of July between 49.6°N and 49.9°N. During the same period, we recorded lower nTA values in these areas, which might be linked to the production of calcium carbonate by the coccolithophores. nTA decreased by nearly 5 to 10 μmol kg^{-1} during this event (Fig. 2f). Instead, an increase in nTA can be linked to the uptake of nitrate by phytoplankton (Brewer and Goldman, 1976): an increase of nTA of 1 mol corresponds to 1 mol of nitrate assimilated by phytoplankton. In the middle of the Channel, the winter stock of nitrate ranged from 6 to 10 μmol L^{-1} (data not shown) and was entirely depleted just after the spring phytoplankton bloom. At the same time we observed an increase of nTA of 5 to 10 μmol kg^{-1} (Fig. 2f), which corresponds to the equi-molar ratio mentioned above. Hence, nitrate depletion seemed to be the main driver of the increase of TA during the productive period. Only when short coccolithophore blooms occurred, calcium carbonate production decreased TA and counteracted the nitrate depletion. Near the coastline TA decreases were essentially driven by freshwater inputs.

In the following sections, we assess the main drivers of the seasonal variability of pCO_2 and air–sea CO_2 fluxes in the two main provinces of the WEC. We particularly focus on the biological and thermodynamic processes.

4.2. Processes controlling the seasonal pCO_2 variability

The high spatio-temporal coverage of our dataset allowed us to assess and compare the processes controlling the seasonal pCO_2 variability in the provinces of the WEC. In western European shelf zone like the English Channel, the main drivers of pCO_2 variability are the thermodynamic and biological production/respiration of organic matter (Padin et al., 2007; Dumousseaud et al., 2010). The pCO_2 values were computed at the annual mean temperature (T_{mean} = 13.1 °C) using CO2SYS (Pierrot et al., 2006) in order to remove the thermal effect on pCO_2 ($pCO_{2,nontherm}$) and assess the biological processes controlling the pCO_2 variability. To evaluate the impact of the temperature on the pCO_2 variability, we computed $pCO_{2,therm}$ according to Eq. (3). Eq. (3) perturbs the annual mean pCO_2 calculated each year with the observed SST. The $pCO_{2,therm}$ represents realistically the seasonal thermal forced pCO_2 variability during the year (Takahashi et al., 2002).

$$pCO_{2,therm} = pCO_{2,mean} \times e^{0.0423 \times (Tobs - Tmean)}. \quad (3)$$

In Eq. (3), "mean" and "obs" stand for annual mean and observed temperatures and pCO_2, respectively. This simple approach to estimate the impact of biological and thermodynamic effects on pCO_2 variations can provide a reasonable assessment of the relative importance of these processes in coastal ecosystems according to Thomas et al. (2005) and Schiettecatte et al. (2006). Besides thermodynamic and production/respiration of organic matter, additional processes like dissolution/formation of $CaCO_3$, lateral advection and horizontal mixing can have an impact on pCO_2 variability. As discussed above, pelagic dissolution and formation of $CaCO_3$ occurred in the north part of the northern WEC in early June and at the end of July. These processes are included in the $pCO_{2,nontherm}$. The short time-steps of our computation (two weeks) was much lower than the flushing time at ASTAN and E1 (30 to 90 days according to Delhez et al., 2004), which makes lateral advection negligible at this site. The impact of mesoscale eddies (Section 2.4) on pCO_2 are very difficult to quantify and therefore it is included in the $pCO_{2,nontherm}$. However, lateral advection in the vicinity of L4 could not be ignored because sudden freshwater inputs can influence the carbonate system properties on time scales lower than 2 weeks. We therefore chose to apply the normalization of pCO_2 at the annual mean temperature and the Takahashi method only in the two main provinces of the WEC, which are the focus of this study. The horizontal mixing term will be discussed below.

In Fig. 5 we quantify the effect of each process on the pCO_2 variability in both provinces. For this we calculated the mean pCO_2, $pCO_{2,nontherm}$ and $pCO_{2,therm}$ every two weeks using the data collected from the vicinity of ASTAN and E1 stations (Fig. 5). These stations are representative of homogenous (ASTAN) and seasonally stratified (E1) systems found in the WEC and in adjacent seas (i.e. the Celtic and Irish Seas, Pingree and Griffiths, 1978). Variability of $pCO_{2,therm}$ followed SST variations over the year. Maximum $pCO_{2,therm}$ values (over 450 μatm) occurred in late July and in August when the SST was highest. The $pCO_{2,therm}$ stayed higher than 450 μatm for more than one month at E1 and just exceeded this level once at ASTAN. The thermal stratification occurring at E1, which maintained the surface waters warmer, explains this longer maximum. At ASTAN and E1 stations the seasonal SST amplitudes of 7.1 °C and 7.9 °C, respectively (Table 2), were equivalent to the $pCO_{2,therm}$ ranges of 120 μatm and 130 μatm, respectively (Fig. 5). During winter, mean SST at E1 was 9.3 °C and was cooler than at ASTAN (9.9 °C). A difference of 0.6 °C would result in a difference of approximately 9 μatm according to Takahashi et al. (1993) and Fig. 5 confirms that during winter the cooling of surface waters at E1 decreased the $pCO_{2,therm}$ values by approximately 10 μatm compared to ASTAN. During this period, the total mean pCO_2 difference between ASTAN and E1 was 20 μatm (Table 2). The additional 10 μatm difference between ASTAN and E1 resulted from higher $pCO_{2,nontherm}$ values at ASTAN than at E1. The CO_2 undersaturation in the northern WEC during winter was therefore driven by cooler surface water and by lower respiration process at E1 than at ASTAN.

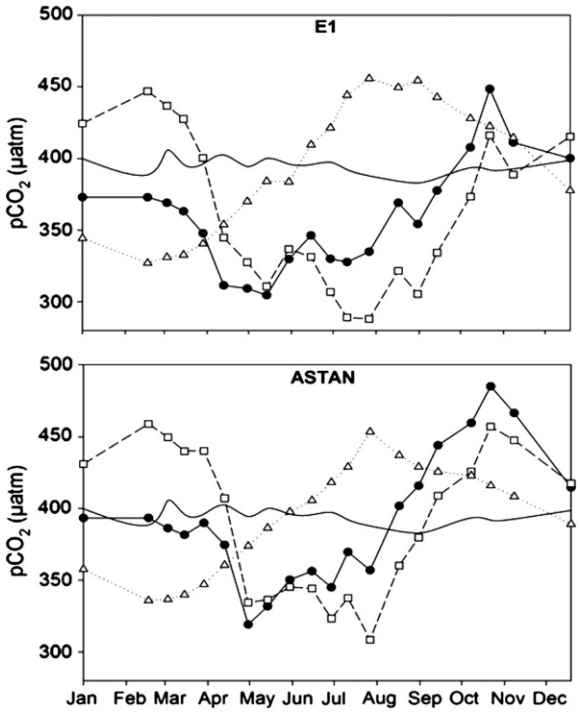

Fig. 5. Variations of pCO_2 (filled circles), $pCO_{2,nontherm}$ (empty squares) and $pCO_{2,therm}$ (empty triangles) in the vicinity of ASTAN and E1 computed after normalization of pCO_2 to the annual mean temperature ($pCO_{2,non\text{-}therm}$) and after Takahashi et al. (1993, 2002) ($pCO_{2,therm}$). The horizontal black lines correspond to pCO_{2air}.

In response to spring phytoplankton blooms the pCO_2 signal was mainly driven by $pCO_{2,nontherm}$ but pCO_2 was compensated by the counteractive thermodynamic influence due to SST increase. The $pCO_{2,nontherm}$ of 350 μatm and 300 μatm recorded from mid-April to mid-August at ASTAN and from April to mid-September at E1 showed that the biological uptake was responsible for the mean CO_2 undersaturations of 50 μatm and 90 μatm observed during this period at ASTAN and E1 respectively. The increase of $pCO_{2,nontherm}$ due to organic matter remineralization started at the end of July at ASTAN and one month later at E1. The increases at ASTAN and at E1 were equivalent to biological releases, which induced CO_2 oversaturations, of approximately 60 μatm and 20 μatm at ASTAN and at E1 respectively. These estimations of the biological respiration of pCO_2 at E1 represent an upper limit since mixing of the water column at E1 might have brought bottom water with higher pCO_2 into the surface waters. Because of the organic matter remineralization, pCO_2 exceeded atmospheric equilibrium in mid-August at ASTAN and in early October at E1. Surface waters stayed oversaturated in CO_2 until the end of the year for ASTAN and E1, with higher pCO_2 values in the homogenous system (>450 μatm) due to the higher remineralization of organic matter compared to the stratified system. As mentioned above in Section 4.1., coccolithophore blooms occurred in the northern WEC in early June (between 49.9°N and 50.2°N) and at the end of July (between 49.6°N and 49.9°N). During these events nTA depletions of 10 μmol kg^{-1} were observed. The theoretical computation of the change of seawater carbonate chemistry speciation related to a TA drawdown of −10 μmol kg^{-1} due to calcification lead to an increase in pCO_2@12.5 °C of 6 μatm. In early June at fixed station E1, we observed a $pCO_{2,nontherm}$ increase of about 10 μatm (Fig. 5), which suggests that calcification processes contributed to half of this increase. In late July, the CO_2 release by calcification processes was compensated by organic carbon production because $pCO_{2,nontherm}$ kept constant between the post coccolithophore bloom and the bloom.

Figs. 2g and 5 confirmed that the biological consumption of pCO_2 started earlier and lasted longer in the northern WEC compared to the southern WEC. Similarly, from the end of summer to the beginning of fall, respiration processes were stronger in the south than in the north of the WEC. $pCO_{2,nontherm}$ and $pCO_{2,therm}$ variability at E1 and ASTAN clearly shows that the thermodynamic effect counteracted consecutively biological production in spring. Comparing these two representative systems (homogenous vs. stratified) of the WEC, our results show that the differences observed between northern and southern WEC were clearly related to the structure of the water column. The control of pCO_2 variability at these stations might be representative of larger provinces of the NW European shelf. For example, the processes driving pCO_2 dynamics in the two provinces of the WEC are likely to exert the same control on pCO_2 dynamics in adjacent Irish (mostly homogeneous) and Celtic (stratified) Seas.

4.3. Air–sea CO_2 exchange

Fig. 6 shows the air–sea CO_2 fluxes calculated during the entire year for each cruise in the two provinces of the WEC and for the area in the vicinity of the 3 fixed stations (ASTAN, E1 and L4). The differences observed between southern and northern WEC and between homogenous and seasonally stratified water column structures (mentioned in Section 3) explained the spatial variability of fluxes of CO_2 across the air–sea interface over the year. Thus, air–sea

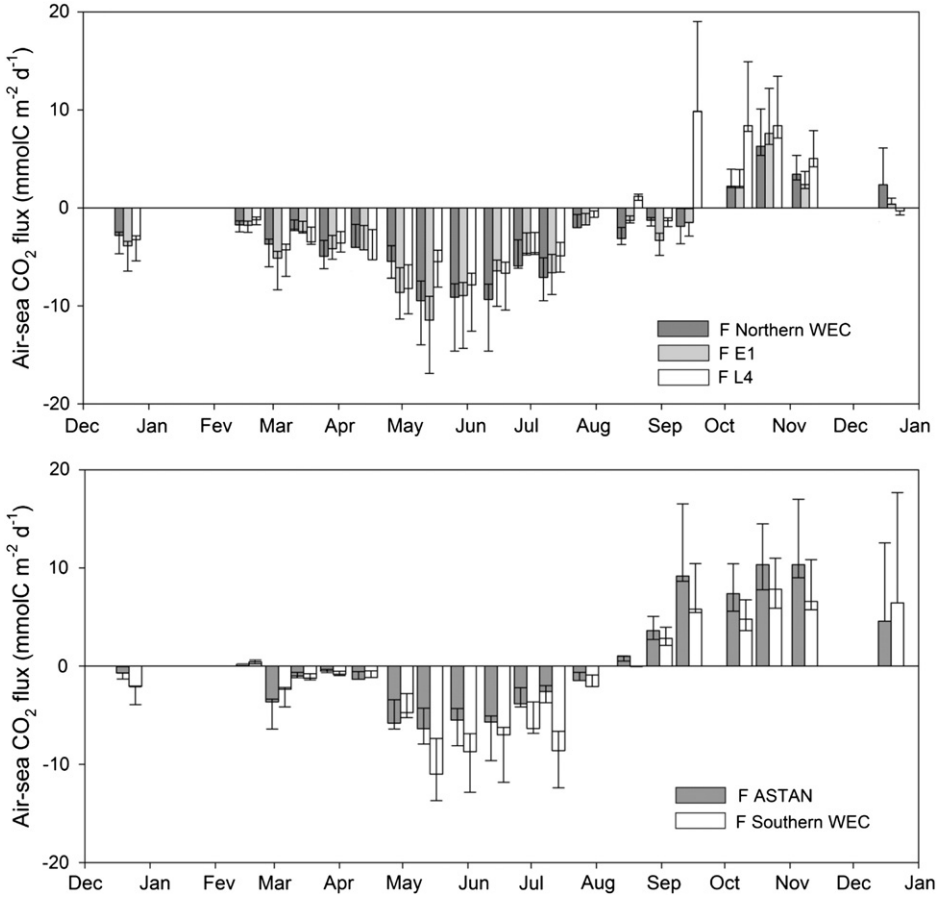

Fig. 6. Calculated air–sea CO_2 fluxes (in mmol C m^{-2} d^{-1}) using the algorithm given by Nightingale et al. (2000), at the fixed station ASTAN, E1 and L4 using VOS data and averaged in the southern WEC (between 48.8°N and 49.5°N) and in the northern WEC (between 49.5°N and 50.3°N). Error bars were computed from the difference obtained between k-wind parameterizations of Nightingale et al. (2000) (N00) and Wanninkhof and McGillis (1999) (W&McG99) for short term winds (ST) and long term (LT) winds. F calculated from W&McG99-ST was generally lower than F computed from N00 and F calculated from W&McG99-LT was generally higher than F computed from N00.

CO_2 fluxes in the southern WEC and at ASTAN had approximately the same dynamics but they differed from F variations in the northern WEC and at E1.

During spring, we found an enhanced oceanic CO_2 sink in the northern WEC and at E1 (mean values of 7.1 and 7.3 mmol m^{-2} day^{-1}, respectively) compared to the southern WEC and ASTAN (mean values of 5.6 and 4.2 mmol m^{-2} day^{-1}, respectively) (Table 5). Significant negative fluxes started around early May in the southern WEC, whereas air–sea CO_2 fluxes were negative from the beginning of the year in the northern WEC (Fig. 6). In the northern province, the presence of subsurface phytoplankton blooms supported by fluorescence profiles made at station E1 (www.westernchannelobservatory.org.uk) from June to August and reported previously by Southward et al. (2005) and by Smyth et al. (2010) may maintain a more important CO_2 sink during summer.

From mid-August to the end of December the southern and permanently well-mixed WEC acted as a source of CO_2 to the atmosphere, whereas the northern and seasonally stratified WEC ecosystem became a source of CO_2 in October and remained oversaturated until December. As discussed above, the late summer CO_2 sink observed in the northern parts of the WEC was mainly driven by the late summer phytoplankton bloom occurring in this area. The CO_2 emissions to the atmosphere during fall (Table 5) were two fold higher in the south and at ASTAN (6.4 and 8.1 mmol m^{-2} day^{-1} respectively) than in the north and at E1 (3.6 and 3.1 mmol m^{-2} day^{-1}). This was due to the important remineralization of organic matter in the well-mixed water column, which induced the strong CO_2 oversaturation observed in this region (Fig. 5).

During winter, the WEC acted as a sink of CO_2 to the atmosphere with uptake values in the northern province 2 to 3 folds higher than in the southern province. The CO_2 sink observed in winter is in disagreement with previous studies from Borges and Frankignoulle (2003) and Dumousseaud et al. (2010), which found CO_2 emissions from January to March. As seen above in Section 4.2., the main driver of this CO_2 sink was the cooling of the surface waters in the northern WEC, which was not captured in these previous studies. However these ecosystems present an important inter-annual variability (as seen from December 2010 and December 2011 data (Fig. 6)), that has to be considered when comparing with previous studies. The remaining seasonal variability (Table 5) was in good agreement with the other studies carried out in the English Channel (Borges and Frankignoulle, 2003; Padin et al., 2007; Dumousseaud et al., 2010; Kitidis et al., 2012).

On an annual scale, ASTAN and the southern WEC were close to atmospheric equilibrium with air–sea CO_2 fluxes values of 0.1 (0.2 0.5) mol m^{-2} y^{-1} and −0.4 (−0.1 −0.3) mol m^{-2} y^{-1} (Table 5), respectively (as indicated in Section 2.3, the values in brackets given for the annual fluxes correspond to those computed from Wanninkhof and McGillis (1999) for short term and long term winds, respectively). The surface waters in the vicinity of ASTAN station can even be considered as a weak source of CO_2 for 2011. E1 and the northern WEC were significant sinks of CO_2 with values of 1.2 (0.8 1.6) mol m^{-2} y^{-1} and 1.1 (0.7 1.4) mol m^{-2} y^{-1}, respectively. These differences can be linked to the different hydrographical structures of the water column, which impacts biological activity and the CO_2 system as detailed above in Section 4.1.

The fact that the permanently well-mixed province of the WEC acted as a weak source of CO_2 to the atmosphere and that the seasonally stratified province of the WEC acted as a significant sink of CO_2 confirms the hypothesis of Borges (2005). This hypothesis stipulates that permanently well mixed systems are less efficient in exporting organic matter and in absorbing atmospheric CO_2, than seasonally or permanently stratified systems. For stations E1 and L4, Kitidis et al. (2012) computed air–sea CO_2 fluxes over four years (2007–2010) of −0.62 ± 0.49 and −0.55 ± 0.66 mol m^{-2} y^{-1}, respectively. We computed air–sea CO_2 fluxes at L4 for comparison with the study of Kitidis et al. (2012). Our flux estimates in 2011 for E1 and L4 were −1.2 (−0.8 −1.6) and −0.5 (−0.3 −0.5) mol m^{-2} y^{-1}, respectively. These results were in relatively good agreement with the study of Kitidis et al. (2012). Our CO_2 sink computed at E1 for 2011 was in the uppermost inter-annual variability of their 2007–2010 estimations (Table 5), although the same k parameterizations (Nightingale et al., 2000) were used in both studies. Our bi-monthly sampling strategy with VOS transects differed from the data acquired monthly by Kitidis et al. (2012) at E1. With this higher sampling frequency, we might have captured more events of CO_2 undersaturation in the surface waters, which would explain our higher annual CO_2 sink at E1. With the VOS line measurements we covered a larger area of the WEC and we observed that massive spring phytoplankton blooms, which were the main driver of the CO_2 sink in the area, were scattered and usually lasted less than 2 weeks. Thus, a major benefit of the VOS line approach was to capture most of the CO_2 variability caused by phytoplankton blooms including the patchiness of these events. For L4, sampling was performed every week by Kitidis et al. (2012) and both estimates were in rather good agreement.

The discrepancies between the fluxes computed at ASTAN and for the southern WEC in this study showed that it can be difficult to find a fixed station representative of an entire province in these dynamic coastal ecosystems. In the context of a global inorganic carbon observatory for coastal ecosystems (Borges et al., 2010), the frequency of sampling at time series is essential for a robust estimate of air–sea CO_2 fluxes. This type of combined approach with VOS line and fixed stations and adequate sampling frequency can provide a robust assessment of the CO_2 dynamics in continental shelf provinces.

Annual air–sea CO_2 flux estimates for the northern and southern WEC presented in this study were in the same range as those reported by Padin et al. (2007), −0.5 ± 1.2 mol m^{-2} y^{-1} and those estimated from Dumousseaud et al. (2010), ranging from −0.6 to 0.3 mol m^{-2} y^{-1} (Table 5). Results obtained by Borges and Frankignoulle (2003) described the WEC as a source of CO_2 to the atmosphere of 0.5 ± 0.6 mol m^{-2} y^{-1}. These results were in agreement with our estimations obtained at ASTAN, which was a weak source of CO_2 for the atmosphere, but were in contradiction with those obtained in the northern WEC and at E1. Borges and Frankignoulle (2003) pointed out that their data were obtained mostly through the middle of the Channel and did not take into account the latitudinal variability of the WEC. The same applies to the studies of Padin et al. (2007) and Dumousseaud et al. (2010) based

Table 5
Seasonal means of air–sea CO_2 fluxes (F in mmol C m^{-2} d^{-1}) calculated in this study according to Eq. (1) for the northern and southern WEC provinces defined by the 49.5 N latitude boundary and at the fixed stations ASTAN, E1 and L4. These fluxes were computed using the gas transfer velocity formulated by Nightingale et al. (2000). Annual means are in mol C m^{-2} y^{-1}. Annual means in brackets were calculated using Wanninkhof & McGillis (1999) k parameterization for short term (first number) and long term (second number) winds. Atmospheric pCO_2 were measured at Mace Head (Ireland) station from the RAMCES network and wind speeds were obtained from the NCEP/NCAR re-analysis project. Also indicated are the air–sea CO2 fluxes from Borges and Frankignoulle (2003) (B & F), Padin et al. (2007) (P et al.), Dumousseaud et al. (2010) (D et al.) and Kitidis et al. (2012) (K et al.). F values from D et al. are the range of F values for each season in the WEC and the annual mean is an estimation based on the seasonal mean values over the years.

	Winter	Spring	Summer	Fall	Annual
FCO2 Northern WEC	−2.6	−7.1	−3.6	3.6	−1.1 (−0.7 −1.4)
FCO2 Southern WEC	−1.3	−5.6	−1.4	6.4	−0.4 (−0.1 −0.3)
FCO2 Astan	−1.3	−4.2	1.0	8.1	0.1 (0.2 0.5)
FCO2 E1	−3.3	−7.3	−3.2	3.1	−1.2 (−0.8 −1.6)
FCO2 L4	−3.1	−6.2	−0.1	5.4	−0.5 (−0.3 −0.5)
FCO2 from B & F		−1		2	0.5
FCO2 from P et al.		−7		1	−0.5
FCO2 from D et al.		−3.5	−2	3	−0.5
FCO2 from K et al. E1	−2.5	−3	−2	1	−0.62
FCO2 from K et al. L4	−2.5	−4	−2	1	−0.55

on transects through the middle of the Channel. Compared to those studies, our dataset gives a new spatio-temporal resolution across the WEC and highlights significant intra-annual differences between homogenous and seasonally stratified systems. The adjacent Irish (mainly homogenous) and Celtic (stratified) Seas, for which data on the carbonate system are sparse, are likely to show similar patterns for CO_2 dynamics as observed in the two provinces of the WEC defined in this study. The WEC with annual air–sea CO_2 fluxes ranging from 0.1 to −1.2 mol m^{-2} y^{-1} in its different provinces can be considered as a minor sink for atmospheric CO_2 compared to the average flux of −1.85 mol m^{-2} y^{-1} computed by Borges et al. (2006) for European continental shelves as a whole.

4.4. Estimation of net ecosystem production at the fixed stations

NEP estimates based on the DIC budgets (Eq. (2)) and air–sea CO_2 fluxes were plotted over the year at ASTAN and E1 stations (Fig. 7). At ASTAN, from March to the end of July, the surface waters were mostly autotrophic (NEP > 0), and became heterotrophic (−16.9 mmol C m^{-2} day^{-1}) around mid-July. During the spring bloom, in late April, the strongest NEP value (126.8 mmol C m^{-2} day^{-1}) was observed at the same time as the minimum air–sea CO_2 exchange value (−6.0 mmol m^{-2} day^{-1}) when ASTAN acted as a strong sink for atmospheric CO_2. From mid-August to the end of the year the ecosystem was heterotrophic (NEP < 0) with values ranging from −95.7 to −6.6 mmol C m^{-2} day^{-1}. During this time ASTAN acted as strong source of CO_2 to the atmosphere due to the remineralization of organic matter. On an annual scale, ASTAN was slightly autotrophic at a rate of 1.0 mol C m^{-2} y^{-1}.

At E1, from March to the end of August, the surface waters were mostly autotrophic with a weak heterotrophic phase around mid-August (−16.1 mmol C m^{-2} day^{-1}). In contrast to ASTAN, we did not observe a peak of NEP during spring blooms at E1 but the autotrophic phase lasted one month longer. During this period, surface waters at E1 acted as a sink for atmospheric CO_2. From early September to the end of the year the surface waters were mostly heterotrophic with a low autotrophic phase around mid-November

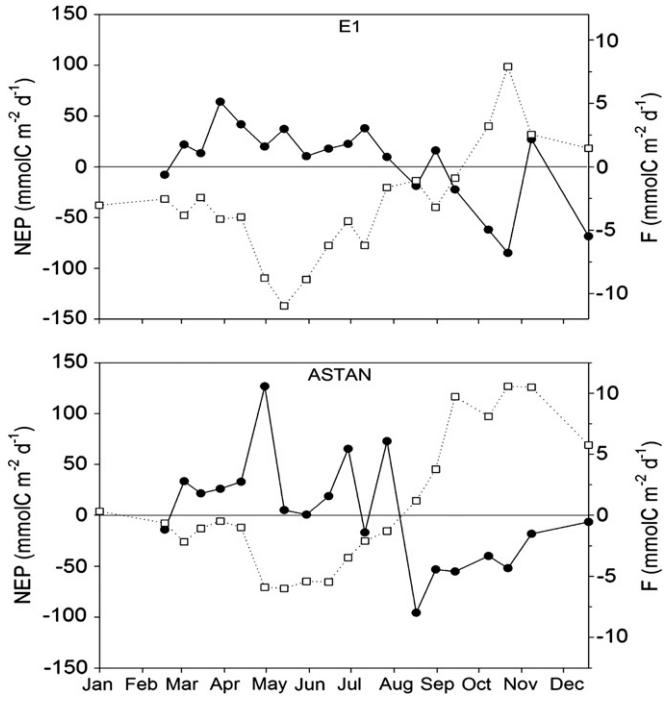

Fig. 7. Estimated net ecosystem production (NEP in mmol C m^{-2} d^{-1}, filled circles) and air–sea CO_2 fluxes (F in mmol C m^{-2} d^{-1}, empty squares) computed using the gas transfer velocity parameterization given by Nightingale et al. (2000) at ASTAN and E1 during the year 2011.

(27.1 mmol C m^{-2} day^{-1}). During this time E1 acted as a source of CO_2 to the atmosphere. On an annual scale, the surface waters at E1 were autotrophic with an annual mean NEP value of 1.5 mol C m^{-2} y^{-1}, 50% higher than in the surface waters at ASTAN (1.0 mol C m^{-2} y^{-1}). For most of the year, the direction of air–sea CO_2 fluxes was clearly related to the trophic status of the mixed layer at both stations ASTAN and E1 (Fig. 7).

As mentioned above in Section 2.4., pelagic and benthic calcification can have a significant impact on NEP assessments based on DIC budget. During the two coccolithophore blooms observed in the WEC in 2011, nTA depletions of 10 μmol kg^{-1} due to calcification lead to a theoretical pCO_2 release of 6 μatm and to a theoretical DIC consumption of 5 μmol kg^{-1}. As explained in Section 3.4., the CO_2 release was insufficient to overcome the CO_2 under-saturation with respect to atmospheric equilibrium and the impact on air–sea CO_2 fluxes remained rather low. Regarding the DIC budget, with a delta DIC of 5 μmol kg^{-1} due to calcification, the impact of the coccolithophore blooms of June and July on our NEP computation would be approximately +2% on the annual mean. Harlay et al. (2010) reported calcification rates during a coccolithophore bloom in the northern Bay of Biscay ranging between 1.4 and 14 mmol $CaCO_3$ m^{-2} day^{-1}. These authors showed that the increase in pCO_2 due to calcification was also insufficient to overcome the under-saturation of CO_2. Benthic calcification is also present in the English Channel, Migné et al. (1998) and Davoult et al. (2009) estimated calcification rates of brittle stars (*Ophiothrix fragilis* and *Acrocnida brachita*, respectively) in the eastern English Channel to 18.6 mmol $CaCO_3$ m^{-2} day^{-1} and to 1.9–2.8 mmol $CaCO_3$ m^{-2} day^{-1} respectively. Such calcification rates lead to the release of CO_2 into the surrounding water and potentially further transfer to the atmosphere from 1.3 to 1.9 mmol C m^{-2} day^{-1} (Davoult et al. (2009)) to 13.2 mmol C m^{-2} d^{-1} (Migné et al. (1998)). Further Golléty et al. (2008) estimated the calcification rate of barnacles in the south part of the WEC (off Roscoff) with values ranging from 13.2 to 49.3 mmol $CaCO_3$ m^{-2} d^{-1}. Several benthic species are present in temperate coastal ecosystems but carbonate system dynamics between benthic fauna and surrounding waters are difficult to quantify considering the diversity of species. Benthic calcification may influence the CO_2 system of the water—column all year in the well mixed area of the WEC and from fall to early spring in the stratified northern WEC. Our NEP assessments might be impacted by pelagic and benthic calcification but, as we observed from pCO_2 variability (Fig. 5), during the spring and summer productive period surface waters remained under-saturated in CO_2, thus mainly controlled by GPP, and a significant sink of CO_2.

To the best of our knowledge, no previous study has assessed NEP in the WEC. Borges and Frankignoulle (2003) referred to the work of Thomas et al. (1999) (and references therein) to assume that NEP can be approximated to new primary production. In well-mixed waters of the WEC, new primary production was estimated at 0.6 mol C m^{-2} y^{-1} according to annual N-assimilation rates using the Redfield C:N ratio reported by Le Corre et al. (1996) and L'Helguen et al. (1996). This new primary production value was of a similar magnitude as our annual mean NEP estimate of 1.0 mol C m^{-2} y^{-1} at ASTAN, but can only serve as a first order comparison. NEP values for the adjacent Southern Bight of the North Sea (SBNS) were computed by Schiettecatte et al. (2007) based on a comprehensive DIC budget in this all-year well mixed system. These authors found an annual mean NEP of 6.3 mol C m^{-2} y^{-1} associated to an annual mean air–sea CO_2 fluxes of −0.7 mol C m^{-2} y^{-1}. These NEP values were much higher than the NEP values found for the WEC in this study. The SBNS differs from WEC in that it receives strong inputs of nutrients and organic and inorganic carbon from several large estuaries (e.g. Scheldt, Rhine/Meuse, Thames) surrounding the North Sea and this might explain the large differences between these NEP estimates. For the adjacent Irish Sea, Gazeau et al. (2004) reported annual NEP values derived by the Land–Ocean Interactions in the Coastal Zone (LOICZ) method for

European sites (from non-conservative fluxes of DIC and dissolved inorganic phosphorus). The Irish Sea is mainly characterized by a permanently mixed water column similar to ASTAN and receives much less estuarine inputs than the SBNS. The NEP value of 0.7 mol C m^{-2} y^{-1} found by these authors for the Irish Sea was in agreement with the NEP computation at ASTAN indicating a trend of weak autotrophy for this kind of permanently mixed system.

5. Concluding remarks

In this study, we investigated the biogeochemical processes controlling CO_2 system dynamics using surface VOS line data. We combined these VOS line data with vertical profiles at fixed stations to assess the hydrographical structure of the water column. This approach proved to be an excellent tool to identify and describe the different processes controlling the dynamics of the CO_2 system parameters. We separated the WEC into two contrasting provinces with regard to the CO_2 dynamics. The seasonally stratified northern WEC showed enhanced biological activities characterized by an extensive autotrophic phase, which maintained the pCO_2 below the atmospheric equilibrium until early fall and acted as sink for atmospheric CO_2 at a rate of 1.1 mol C m^{-2} y^{-1}. The permanently well mixed southern WEC was characterized by a shorter autotrophic phase due to a delayed spring phytoplankton growth and an early start of the fall heterotrophic phase, resulting in an annual air–sea CO_2 flux close to neutral at a rate of -0.4 mol C m^{-2} y^{-1}. Our latitudinal approach resolved the discrepancy between the directions of the fluxes in the WEC observed in previous studies by differentiating between the hydrological regions.

Our study showed that for such systems, a combined approach, based on VOS line and fixed stations can provide a robust assessment of air–sea CO_2 fluxes in these regions. Indeed, VOS lines surface data alone hamper complete assessment of the processes driving air–sea CO_2 fluxes since they do not provide any information on the hydrological properties of the ecosystems explored. Nowadays, many coastal scientific institutes support coastal observatory networks in their adjacent coastal seas where common biogeochemical parameters (temperature, salinity, DIC, TA, O_2) are measured and available at fixed stations. VOS routes should be established in these marginal seas and, as demonstrated in our study, would allow comprehensive assessments of the processes driving air–sea CO_2 fluxes. This combined approach could be applied in similar contrasting continental shelf systems, and notably in the adjacent stratified/homogenous Celtic and Irish Seas, for which such data on the CO_2 system are sparse.

Acknowledgments

We thank the B.A.I. Brittany Ferry Company for providing access to their vessels and especially the captains and crew of the *Armorique* ferry for their hospitality and their assistance on all the crossings. Additional thanks go to the -4H- JENA team for their technical support with the FerryBox. We acknowledge the work of the Western Channel Observatory funded under the National Capability of the UK Natural Environmental Research Council for the E1 and L4 data. We thank the "Service d'Observation en Milieu Littoral (SOMLIT), INSU-CNRS" from the biological station of Roscoff for the ASTAN data. We are grateful to the SNAPO-CO_2 (Service National d'Analyse des paramètres Océaniques du CO_2) lab for assistance with the DIC/TA analysis. We thank M. Ramonet for making available the atmospheric pCO_2 data from the RAMCES network (Observatory Network for Greenhouse Gases), the SHOM "Service Hydrographique et Oceanographique de la Marine" for assistance with the salinity analysis and to X.A. Padin for his help relative to the NCEP/NCAR wind data. We thank A.C. Baudoux and I. Probert for their help in previous versions of the manuscript. We thank the associated editor and the two anonymous reviewers for their constructive comments on previous versions of the manuscript. This work was partly funded by the Project INTERREG IV/MARINEXUS and by the "Region Bretagne" (program ARED, project CHANNEL). P.M. holds a PhD grant from the Region Bretagne at the UPMC and Y.B. is an associate researcher (CR1) at CNRS.

References

Borges, A.V., Frankignoulle, M., 2003. Distribution of surface carbon dioxide and air–sea exchange in the English Channel and adjacent areas. J. Geophys. Res. Oceans 108 (C5). http://dx.doi.org/10.1029/2000JC000571.

Borges, A.V., 2005. Do we have enough pieces of the jigsaw to integrate CO_2 fluxes in the coastal ocean? Estuaries 28 (1), 3–27.

Borges, A.V., Schiettecatte, L.S., Abril, G., Delille, B., Gazeau, E., 2006. Carbon dioxide in European coastal waters. Estuarine Coastal Shelf Sci. 70 (3), 375–387.

Borges, A.V., Ruddick, K., Schiettecatte, L.-S., Delille, B., 2008. Net ecosystem production and carbon dioxide fluxes in the Scheldt estuarine plume. BMC Ecol. 8, 15. http://dx.doi.org/10.1186/1472-6785-8-15.

Borges, A., et al., 2010. A global sea surface carbon observing system: inorganic and organic carbon dynamics in coastal oceans. In: Hall, J., Harrison, D.E., Stammer, D. (Eds.), Proceedings of OceanObs'09: Sustained Ocean Observations and Information for Society (Vol. 2). ESA Publication WPP-306 (Venice, Italy, 21–25 September 2009).

Bozec, Y., Thomas, H., Schiettecatte, L.S., Borges, A.V., Elkalay, K., de Baar, H.J.W., 2006. Assessment of the processes controlling seasonal variations of dissolved inorganic carbon in the North Sea. Limnol. Oceanogr. 51 (6), 2746–2762.

Brewer, P.G., Goldman, J.C., 1976. Alkalinity changes generated by phytoplankton growth. Limnol. Oceanogr. 21 (1), 108–117.

Chen, C.T.A., Borges, A.V., 2009. Reconciling opposing views on carbon cycling in the coastal ocean: continental shelves as sinks and near-shore ecosystems as sources of atmospheric CO_2. Deep-Sea Res. II Top. Stud. Oceanogr. 56 (8–10), 578–590.

Davoult, D., Harlay, J., Gentil, F., 2009. Contribution of a dense population of the brittle star. *Acrocnida brachiata* (Montagu) to the biogeochemical fluxes of CO_2 in a temperate coastal ecosystem. Estuar. Coasts 32, 1103–1110.

Delhez, E.J.M., Heemink, A.W., Deleersnijder, E., 2004. Residence time in a semi-enclosed domain from the solution of an adjoint problem. Estuarine Coastal Shelf Sci. 61 (4), 691–702.

Dickson, A.G., Millero, F.J., 1987. A comparison of the equilibrium constants for the dissociation of carbonic acid in seawater media. Deep Sea Res. Part A 34 (10), 1733–1743.

Dumousseaud, C., Achterberg, E.P., Tyrrell, T., Charalampopoulou1, A., Schuster, U., Hartman, M., Hydes, D.J., 2010. Contrasting effects of temperature and winter mixing on the seasonal and inter-annual variability of the carbonate system in the Northeast Atlantic Ocean. Biogeosciences 7 (5), 1481–1492.

EPA, 1997. In Vitro Determination of Chlorophyll a and Pheophytin a in Marine and Freshwater Algae by Fluorescence (Arar E.J. & Collins G.B.). Method 445.0, revision 1.2. US Environmental Protection Agency, Cincinnati (26 pp.).

Friis, K., Körtzinger, A., Wallace, D.W.R., 2003. The salinity normalization of marine inorganic carbon chemistry data. Geophys. Res. Lett. 30 (2). http://dx.doi.org/10.1029/2002GL015898.

Garcia-Soto, C., Fernandez, E., Pingree, R.D., Harbour, D.S., 1995. Evolution and structure of a shelf coccolithophore bloom in the Western English Channel. J. Plankton Res. 17 (11), 2011–2036.

Gattuso, J.P., Frankignoulle, M., Wollast, R., 1998. Carbon and carbonate metabolism in coastal aquatic ecosystems. Annu. Rev. Ecol. Evol. Syst. 29, 405–434.

Gazeau, F., Smith, S.V., Gentili, B., Frankignoulle, M., Gattuso, J.P., 2004. The European coastal zone: characterization and first assessment of ecosystem metabolism. Estuarine Coastal Shelf Sci. 60 (4), 673–694.

Gazeau, F., Borges, A.V., Barrón, C., Duarte, C.M., Iversen, N., Middelburg, J.J., Delille, J.J., Pizay, M.D., Frankignoulle, M., Gattuso, J.P., 2005. Net ecosystem metabolism in a micro-tidal estuary (Randers Fjord, Denmark): evaluation of methods. Mar. Ecol. Prog. Ser. 301, 23–41.

Golléty, C., Gentil, F., Davoult, D., 2008. Secondary production, calcification and CO_2 fluxes in the cirripedes *Chthamalus montagui* and *Elminius modestus*. Oecologia 155 (1), 133–142.

Harlay, J., Borges, A.V., Van Der Zee, C., Delille, B., Godoi, R.H.M., Schiettecatte, L.-S., Roevros, N., Aerts, K., Lapernat, P.-E., Rebreanu, L., Groom, S., Daro, M.-H., Van Grieken, R., Chou, L., 2010. Biogeochemical study of a coccolithophore bloom in the northern Bay of Biscay (NE Atlantic Ocean) in June 2004. Prog. Oceanogr. 86, 317–336.

Hill, A.E., Brown, J., Fernand, L., Holt, J., Horsburgh, K.J., Proctor, R., Raine, R., Turrell, W.R., 2008. Thermohaline circulation of shallow tidal seas. Geophys. Res. Lett. 35 (11). http://dx.doi.org/10.1029/2008GL033459 (L11605).

Kalnay, E., Kanamitsu, M., Kistler, R., Collins, W., Deaven, D., Gandin, L., Iredell, M., Saha, S., White, G., Woollen, J., Zhu, Y., Chelliah, M., Ebisuzaki, W., Higgins, W., Janowlak, J., Mo, K.C., Ropelewski, C., Wang, J., Leetmaa, A., Reynolds, R., Jenne, R., Joseph, D., 1996. The NCEP/NCAR reanalysis project. Bull. Am. Meteorol. Soc. 77, 437–471.

Kelly Gerreyn, B.A., Hydes, D.J., Fernand, L.J., Jegou, A.M., Lazure, P., Puillat, I., García-Soto, C., 2006. Low salinity intrusions in the western English Channel. Cont. Shelf Res. 26 (11), 1241–1257.

Kitidis, V., Hardman-Mountford, N.J., Litt, E., Brown, I., Cummings, D., Hartman, S., Hydes, D., Fishwick, J.R., Harris, C., Martinez-Vicente, V., Malcolm, E., Woodward, S., Smyth, T.J., 2012. Seasonal dynamics of the carbonate system in the Western English Channel. Cont. Shelf Res. 42, 30–40.

L'Helguen, S., Madec, C., Le Corre, P., 1996. Nitrogen uptake in permanently well-mixed temperate coastal waters. Estuarine Coastal Shelf Sci. 42 (6), 803–818.

Le Corre, P., Wafar, M., L'Helguen, S., Maguer, J.F., 1996. Ammonium assimilation and regeneration by size-fractionated plankton in permanently well-mixed temperate waters. J. Plankton Res. 18 (3), 355–370.
Mehrbach, C., Culberso, Ch., Hawley, J.E., Pytkowic, R.M., 1973. Measurement of apparent dissociation constants of carbonic acid in seawater at atmospheric pressure. Limnol. Oceanogr. 18 (6), 897–907.
Migné, A., Davoult, D., Gattuso, J.-P., 1998. Calcium carbonate production of a dense population of the brittle star *Ophiothrix fragilis* (Echinodermata: Ophiuroidea): role in the carbon cycle of a temperate coastal ecosystem. Mar. Ecol. Prog. Ser. 173, 305–308.
Monterey, G., Levitus, S., 1997. Seasonal variability of mixed layer depth for the world ocean. NOAA Atlas, NESDIS 14, Washington D.C. (96 pp.).
Nightingale, P.D., Malin, G., Law, C.S., Watson, A.J., Liss, P.S., Liddicoat, M.I., Boutin, J., Upstill-Goddard, R.C., 2000. In situ evaluation of air-sea gas exchange parameterizations using novel conservative and volatile tracers. Global Biogeochem. Cycles 14 (1), 373–387.
Odum, H.T., 1956. Primary production in flowing waters. Limnol. Oceanogr. 1 (2), 102–117.
Padin, X.A., Vazquez-Rodriquez, M., Rios, A.F., Perez, F.F., 2007. Surface CO_2 measurements in the English Channel and Southern Bight of North Sea using voluntary observing ships. J. Mar. Syst. 66 (1–4), 297–308.
Pierrot, D., Lewis, E., Wallace, D.W.R., 2006. MS Excel Program Developed for CO_2 System Calculations. ORNL/CDIAC-105. Carbon Dioxide Information Analysis Center, Oak Ridge National Laboratory, U.S. Department of Energy, Oak Ridge, Tennessee.
Pingree, R.D., Griffiths, D.K., 1978. Tidal fronts on shelf seas around British isles. J. Geophys. Res. Oceans Atmos. 83 (NC9), 4615–4622.
Reid, P.C., Auger, C., Chaussepied, M., Burn, M. (Eds.), 1993. The Channel, Report on Sub-Region 9, Quality Status Report of the North Sea 1993. UK Dep. of the Environ., Républ. Fr. Minist. de l'Environ., Inst. Fr. de Rech. Pour l'Exploit. de la Mer, Brest (153 pp.).
Schiettecatte, L.S., Gazeau, F., van der Zee, C., Brion, N., Borges, A.V., 2006. Time-series of the partial pressure of carbon dioxide (2001–2004) and preliminary inorganic carbon budget in the Scheldt plume (Belgian coastal waters). Geochem. Geophys. Geosyst. 7. http://dx.doi.org/10.1029/2005GC001161.
Schiettecatte, L.S., Thomas, H., Bozec, Y., Borges, A.V., 2007. High temporal coverage of carbon dioxide measurements in the Southern Bight of the North Sea. Mar. Chem. 106 (1–2), 161–173.
Smyth, T.J., Fishwick, J.R., Al-Moosawi, L., Cummings, D.G., Harris, C., Kitidis, V., Rees, A., Martinez-Vicente, V., Woodward, E.M.S., 2010. A broad spatio-temporal view of the Western English Channel observatory. J. Plankton Res. 32 (5), 585–601.
Southward, A.J., et al., 2005. Long-term oceanographic and ecological research in the western English Channel. Adv. Mar. Biol. 47, 1–105.
Takahashi, T., Olafsson, J., Goddard, J.G., Chipman, D.W., Sutherland, S.C., 1993. Seasonal variation of CO_2 and nutrients in the high-latitude surface ocean — a comparative study. Global Biogeochem. Cycles 7 (4), 843–878.
Takahashi, T., et al., 2002. Global sea–air CO_2 flux based on climatological surface ocean pCO_2, and seasonal biological and temperature effects. Deep-Sea Res. II Top. Stud. Oceanogr. 49 (9–10), 1601–1622.
Thomas, H., Ittekkot, V., Osterroht, C., Schneider, B., 1999. Preferential recycling of nutrients — the ocean's way to increase new production and to pass nutrient limitation? Limnol. Oceanogr. 44 (8), 1999–2004.
Thomas, H., Bozec, Y., Elkalay, K., de Baar, H.J.W., 2004. Enhanced open ocean storage of CO_2 from shelf sea pumping. Science 304 (5673), 1005–1008.
Thomas, H., Bozec, Y., Elkalay, K., De Baar, H., Borges, A., Schiettecatte, L.-S., De Baar, H.J.W., 2005. Controls of the surface water partial pressure of the CO_2 in the North Sea. Biogeosciences 2, 323–334.
Wafar, M.V.M., Le Corre, P., Birrien, J.L., 1983. Nutrients and primary production in permanently well-mixed temperate coastal waters. Estuarine Coastal Shelf Sci. 17 (4), 431:446.
Walsh, J.J., 1991. Importance of continental margins in the marine biogeochemical cycling of carbon and nitrogen. Nature 350 (6313), 53–55.
Walsh, J.J., Rowe, G.T., Iverson, R.L., McRoy, C.P., 1981. Biological export of shelf carbon is a sink of the global CO_2 cycle. Nature 291 (5812), 196–201.
Wanninkhof, R., McGillis, W.R., 1999. A cubic relationship between air–sea CO_2 exchange and wind speed. Geophys. Res. Lett. 26 (13), 1889–1892.
Weiss, R.F., 1970. Solubility of nitrogen, oxygen and argon in water and seawater. Deep-Sea Res. 17 (4), 721–735.
Weiss, R.F., Price, B.A., 1980. Nitrous oxide solubility in water and seawater. Mar. Chem. 8, 347–359.
Widdicombe, C.E., Eloire, D., Harbour, D., Harris, R.P., Somerfield, P.J., 2010. Long-term phytoplankton community dynamics in the Western English Channel. J. Plankton Res. 35 (5), 643–655.
Wolf-Gladrow, D.A., Zeebe, R.E., Klaas, C., Koertzinger, A., Dickson, A.G., 2007. Total alkalinity: the explicit conservative expression and its application to biogeochemical processes. Mar. Chem. 106 (1–2), 287–300.
Zeebe, R.E., Wolf-Gladrow, D.A., 2001. CO_2 in seawater: equilibrium, kinetics, isotopes. Elsevier Oceanography Series 65. Elsevier, Amsterdam, p. 346.